Embedding Invisible Codes into Normal Video Projection: Principle, Evaluation and Applications

Jingwen Dai, *Student Member, IEEE,* and Ronald Chung, *Senior Member, IEEE*

Abstract

We describe a system of embedding codes into projection display for structured light based sensing, with the purpose of letting projector serve as both a display device and a 3D sensor. The challenge is to make the codes imperceptible to human eyes so as not to disrupt the content of the original projection. There is the temporal resolution limit of human vision that one can exploit, by having a higher than necessary frame rate in the projection and stealing some of frames for code projection. Yet there is still the conflict between imperceptibility of the embedded codes and the robustness of code retrieval that has to be addressed. We introduce noise-tolerant schemes to both the coding and decoding stages. At the coding end, specifically designed primitive shapes and large Hamming distance are employed to enhance tolerance toward noise. At the decoding end, pre-trained primitive shape detectors are used to detect and identify the embedded codes – a task difficult to achieve by segmentation that is used in general structured light methods, for the weakly embedded information is generally interfered by substantial noise. Extensive experiments including evaluations of code imperceptibility, decoding accuracy and sensitivity analysis show that the proposed system is effective, even with the prerequisite of incurring minimum disturbance to the original projection.

Index Terms

imperceptible structured light sensing, embedded pattern design, primitive shape detection and classification, sensitivity analysis

I. Introduction

The improving performance, declining price, and diminishing size of digital video projectors make it possible to use them prevalently. Being able to generate arbitrarily large display is a feature of projectors that makes them exceedingly attractive, especially in applications that demand portability. On the other hand, the adoption of structured light illumination has been proven to be an effective and accurate means for 3D information perception [1]. Recently, the availability of pico projectors with average dimensions of $4 \times 2 \times 1$ inches has widely extended the application domain of structured light system. There are already pocket DCs, DVs and cellular phones (as shown

J. Dai and R. Chung are with the Department of Mechanical and Automation Engineering, The Chinese University of Hong Kong, Shatin, NT, Hong Kong. e-mail: {jwdai, rchung}@mae.cuhk.edu.hk

in Fig. 1) in the consumable market that have both projector and camera built-in, making it possible to implement structured light system in hand-held consumer electronic products.

Fig. 1. Mobile devices with built-in pico projector.

In other words, projector accompanied by camera has the potential of achieving both display and sensing, i.e., for both input and output in human-computer interface, making it a possible device to replace traditional LCD panel, keyboard, and touch-sensitive screen altogether in computing, with only diminished size and weight. Projector has the potential of making a breakthrough of dramatically downsizing portable computing without sacrificing display size.

For these reasons projector-camera (ProCam) system has been actively researched in the last few years. Many research groups apply projectors in unconventional ways to develop new and innovative information displays that go beyond simple screen presentations [2].

Some researchers designed structured light system in the non-visible spectrum [3]. That way the media for regular projection and structure light based sensing (SLS) can be made separate. However, additional hardware could be reduced and device size diminished if structured light and regular projection can be achieved through the same projector. This leads to the concept of Imperceptible Structured Light (ISL). ISL modulates the projected display either spatially or temporally to embed code patterns for structured light based sensing. In principle, due to limitation of human visual perception, the embedded code patterns can be made undetectable to the user, but cameras synchronized to the modulation are able to reconstruct the embedded codes for SLS.

The embedding of code patterns into regular projection can be used for a variety of applications including projector calibration, camera tracking, and 3D scanning.

There is however challenge in embedding codes into regular projection. While the codes should be made as undetectable as possible to the user, they have to be decodable to the camera for the purpose of SLS. On top of the dilemma, there is the inevitable fact that the displayed signals are generally corrupted by substantial noise that arises from the nonlinearity of the projector, the sensing defects of the camera, and the variation of the ambient

illumination. The objective of this work is to deal with the dilemma and the accompanying issues.

This article describes a novel method of embedding imperceptible structured codes into arbitrarily intended projection. Through precise projector-camera synchronization, structured codes consisting of three primitive shapes are embedded into the projection, in a way that is imperceptible to viewers but extractable from the "difference image" between successive images captured by a camera. To make the decoding process more robust against noise, we do not extract the codes by region segmentation in the image domain. Instead we employ specially trained classifiers to detect and identify the codes. To enhance the error tolerance further, specially designed primitive shapes and large Hamming distance are adopted in the spatial coding. Even with some bits of the codewords missed or wrongly coded, the correct correspondence could still be derived correctly.

The remainder of this paper is structured as follows. In Section II, related works on imperceptible structured light sensing are briefly reviewed. The principle of embedding imperceptible codes along with robust coding and a noise-tolerant decoding mechanism are described in Section III. In Section IV, system setup and experimental results are shown. Conclusion and possible future work are offered in Section VII.

II. RELATED WORK

A proof of concept for embedding invisible structured light patterns into DLP (Digital Light Processing) projections first appeared in the "Office of the Future" project [4]. In this work, binary codes are embedded by projecting temporally alternating code images and their complements. Provided that the frequency of projection reaches the *flicker fusion threshold* ($\geq 75Hz$), the pattern and the inverse pattern are visually integrated over time in human perception, and the illumination has the appearance of a flat field ("white" light) to humans. However, the demonstration required significant modification effort on the projection hardware and firmware, including removal of the color wheel and reprogramming of the controller. The resulting images were also in greyscale only. The implementation of such a setting was impossible without mastering and full access to the projection hardware.

Cotting et. al. introduced a coding scheme [5] that synchronizes a camera to a specific time slot of a DLP micro-mirror flipping sequence in which imperceptible binary patterns are embedded. However, not all mirror states are available for all possible intensities, and the additional hardware, DVI repeater with tapped vertical sync signal, is not an off-the-shelf instrument.

However, with the development of digital projection technology, some so-called 3D compatible DLP projectors with refresh rate of $120Hz$ or higher emerged recently. This makes it possible to implement imperceptible structured light without any hardware modification or extra assisting hardware. Many researcher began to study how to determine the embedded intensity properly to guarantee code imperceptibility.

In [6], subjective evaluation results and statistical analysis on the visual perceptibility of embedded codes in different ways were reported. The factors affecting code visibility are also outlined. Park et al. [7] presented a technology for adaptively adjusting the intensity of the embedded code with the goal of minimizing its visibility. It was regionally adapted depending on the spatial variation of neighboring pixels and their color distribution in the YIQ color space. The final code intensity was then weighted by the estimated local spatial variation. Since

two manually defined parameters adjusted the overall strength of the integrated code, the system was not able to automatically calculate an optimized intensity. Grundhofer et al. [8] proposed a method considering the capabilities and limitations of human visual perception for embedding codes. It estimated the Just Noticeable Differences (JND) based on the human contrast sensitivity function and adapted the code intensity on the fly through regional properties of the projected image and code, such as luminance and spatial frequencies. The shortcoming of this method was that some parameters need be pre-measured using some optical devices (e.g. photometer), which were not accessible to nonprofessional users.

To the best of our knowledge, up to now, few works focus on the decoding method in imperceptible code embedding configuration, especially when huge external noise could exist.

III. THE METHOD

A. Principle of Embedding Imperceptible Codes

The fundamental principle behind imperceptible structured code embedding is the temporal integration achieved by projecting each image twice at high frequency: a first image containing actual code information (e.g., by adding or subtracting a certain amount (Δ) to or from the pixels of the original image, depending upon the code) and a second image that compensates for the distortion in the first image. The vital aspects of ISL sensing are code embedding and projector-camera synchronization.

Since general projection is in color, it is possible to embed color code through three different channels. However, to enhance code robustness toward noise, we use binary code and embed it into all three color channels simultaneously. Let B, O, I and I' be the binary code image, the original image, the projected image, and the complementary image respectively. Then the projected image and complementary image could be formulated as

$$I_i(x,y) = O_i(x,y) + P(x,y), \tag{1}$$

$$I'_i(x,y) = O_i(x,y) - P(x,y), \tag{2}$$

$$P(x,y) = \begin{cases} \Delta, & when \quad B(x,y) = 1; \\ 0, & when \quad B(x,y) = 0. \end{cases} \tag{3}$$

where i = {R,G,B} indicates red, green and blue channels, Δ is the embedded intensity.

To avoid intensity saturation at lower and higher intensity levels when adding or subtracting Δ, the original image needs to have the intensity range in each color channel compressed to between Δ to $255 - \Delta$. Since the embedded intensity required in the coding is small enough, the visual degradation due to contrast reduction is negligible.

The degree of imperceptibility thus depends upon the embedded intensity. A larger intensity enables the code to be more tolerant toward noise and more readable in the image of the projection, whilst a smaller intensity makes the embedded codes more invisible. In our design, code imperceptibility has higher priority, and thus embedded intensity is set to a very small value.

In order to achieve imperceptible structured light projection, the frequency of projection must exceed the flicker fusion threshold, which is $75Hz$ for most of the people. Here we take one projection-capture cycle as an example

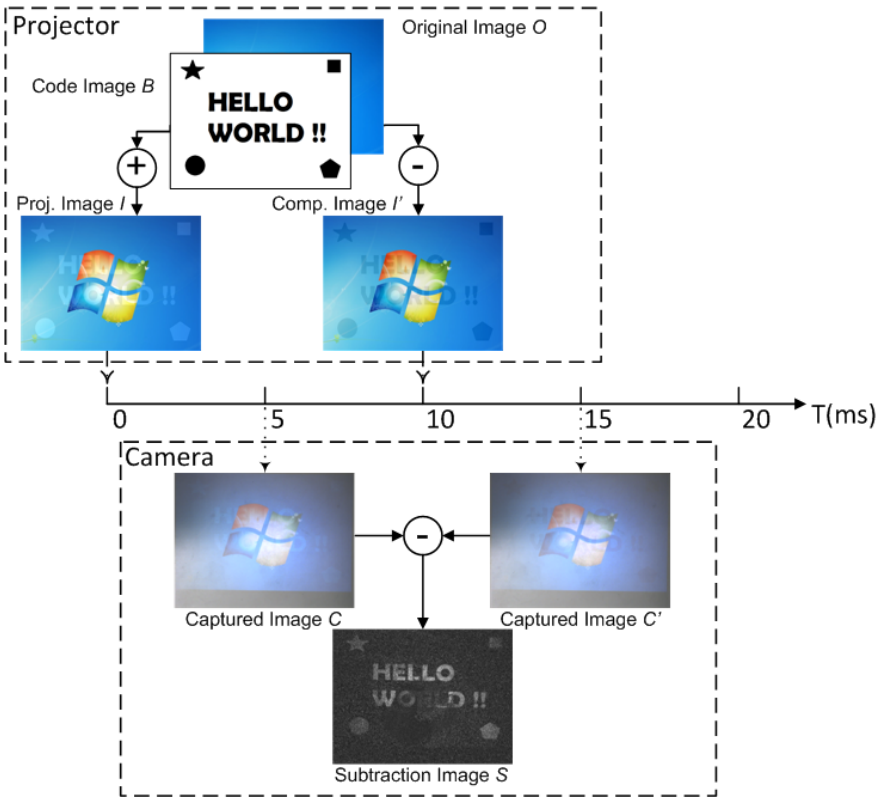

Fig. 2. Projector-camera synchronization and basic principle of embedding and extracting imperceptible codes.

to elaborate the strategy of projector-camera synchronization, which is illustrated in Fig. 2. Firstly, we ensure that the projector projects an image every $10ms$, i.e., at $100Hz$. As shown in Fig. 2, along the time axis, the projected image I and the complementary image I' are projected at the time instants $0ms$, $10ms$ respectively. With a refresh rate of the camera at about 100 frames per second, the camera captures the image C and C' at $5ms$ and $15ms$, shortly after the projector projects the projected image and complementary image to the scene. At $20ms$ a new projection-capture cycle will resume. With the aforementioned projection-capture strategy, the system could capture 50 image pairs per second.

The embedded codes could be internally and simply extracted from the "subtraction image"[1] between consecutively captured images as

$$S(x,y) = \max_i [C_i(x,y) - C'_i(x,y)], \quad i = \{R,G,B\}. \tag{4}$$

Ideally, the subtraction image should be a binary image that has maximum value of 2Δ and minimum value of 0. However, the subtraction image in reality is generally disturbed by large external noises. Since the embedded intensity is always small, the subtraction image has low signal-to-noise ratio. It is generally nontrivial to retrieve the

[1]All the subtraction images in this article are scaled to [0, 255] for illustration purpose.

(a) (b) (c)

Fig. 3. The primitive shapes: (a) cross, (b) sandglass, (c) rhombus.

embedded codes. In the rest of this section, we describe how robust coding and noise-tolerant decoding approaches can help tackle the issue.

B. Design of Embedded Pattern

The strategy of encoding in general structured light methods could be classified into two categories [1]: time multiplexing and spatial multiplexing. The former can achieve denser data samples with higher accuracy, but at the expense of requiring multiple illuminations and image captures over time, which is not suitable for imperceptible code embedding [6] and dynamic scenes. In contrast, the latter labels each pattern position by the appearance profile (color, shape or their combination) of the neighboring positions. The appearance profile can be about various gray levels, colors, or geometric primitives, and the coding methods include De-Bruijn sequences [9], [10], [11], M-arrays [12], [13], [14], [15], and non-formal coding [16], [17], [18], [19]. The spacial coding scheme has the advantage that 3D determination could be achieved with a single pattern.

Considering the constraints of imperceptible code embedding, we employ the spatial multiplex scheme to design our pattern. Due to the choice of using binary code for robust code embedding, the symbols cannot be coded with different colors. We thus use an alphabet set comprising three different geometrical primitives: cross, sandglass, and rhombus, as shown in Fig. 3. There are three advantages of this configuration. First, all the shapes own a natural center point, which simplifies the shape identification process in the decoding stage. Then, there are sufficient variations between different shapes; even with large disturbance from noise on the shapes, the decoding method could discriminate them. Moreover, the directional information carried by the cross shape could rectify the observation window in the step of neighborhood detection without the need of enforcing any other constraint.

In the decoding stage, the centroid of each detected primitive would be considered as the feature point position, and the 9-bit codeword associated to each feature point is composed of the elements in the 3×3 window centered on it. In traditional structured light methods, the uniqueness of the codeword is usually assured by M-arrays (perfect maps), which are random arrays of dimensions $r \times v$ in which a sub-matrix of dimensions $n \times m$ appears only once in the whole pattern [12]. The M-arrays give a total of $rv = 2^{nm} - 1$ unique sub-matrices in the pattern and a window property of $n \times m$. However, the Hamming distance between the codewords is 1, which is generally too small for our code embedding scenario in which the codeword retrieval errors could be large due to noise. In our system, we generate a matrix of dimensions 27×29 using the method proposed by Albitar [20], in which 95.97% of the codewords have a Hamming distance higher than 3 and the average Hamming distance is $\bar{H} = 6.0084$, so that even some bits in the codeword are missed or incorrectly coded, the codeword is still distinguishable. On the

basis of this matrix, the binary code image composed of the primitive shapes appears like the one illustrated in Fig. 4, in which the size of each primitive shape is a collection of 11×11 pixels while the interval between each shape is 11 pixels. The total number of feature points is 783.

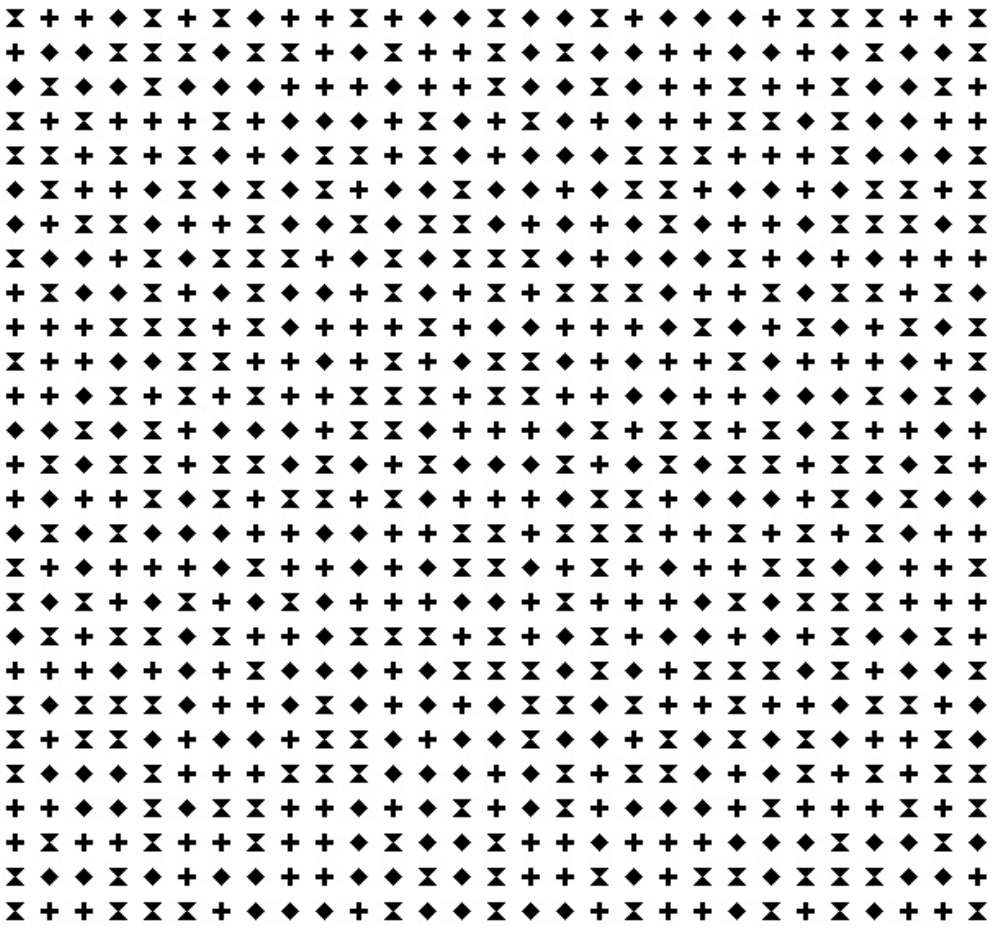

Fig. 4. The embedded binary code image.

C. Primitive Shape Identification and Decoding

In the decoding stage, the existence of intense noises (from projector projection, camera sensing, ambient illumination and object surface reflection influence) makes it impossible to segment the primitive shape by the integrated use of region segmentation and edge or contour detection as often employed in ordinary structured light methods. Here, we regard the primitive shapes as objects to ”identify” and ”detect” rather than ”segment”.

Compared with other object identification or recognition methods, the machine learning approach proposed by P. Viola [21] has been shown to be capable of processing images rapidly with high detection rates for visual object detection. The approach is adopted here for training detector to identify the three primitive shapes. Below we use cross shape as an example to describe the procedure of detector training.

The performance of training-based detector has a great deal to do with the availability of training samples. Unlike generic objects like human face, body or vehicle, which have a large number of samples in a great many of public databases, we have to collect the specific training samples ourselves in the required configuration. 500 color images with different contents were collected from Google Image [22], and 40 cross shapes were embedded in those images at different positions to generate 500 pairs of projected images and complementary images.

A white planar projection screen was placed in front of the projector-camera system with the distance of $800mm$, the orientation of the screen was adjusted to make the projection area appear as a rectangle, i.e. the projection screen was parallel to the projection plane of the projector. By projecting the images, 500 subtraction images could be derived from image capture exercises. The sub-images containing cross shapes were then segmented by manual labeling, which were considered as positive training samples. The background images with holes filled by random noise were divided into small patches to generate negative training samples. The training sample preparation process is shown in Fig. 5.

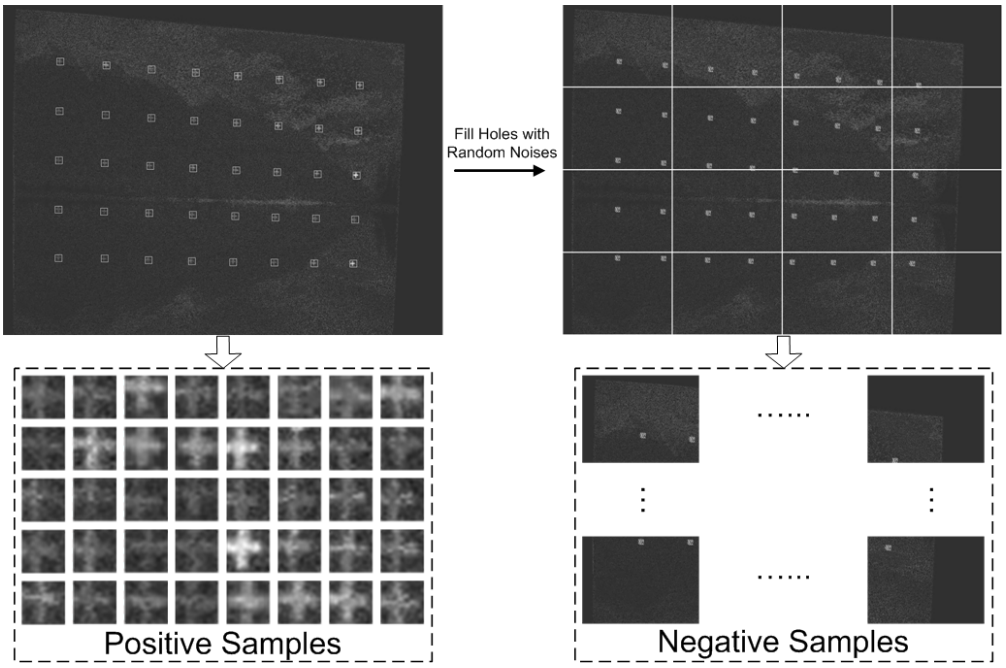

Fig. 5. Training sample preparation.

To obtain the optimal performance, the positive samples were resized to 20×20, the extended haar-like features and Gentle Adaboost algorithm were employed, following the suggestion in [23]. Eventually, from over 7000 positive samples and 3000 negative samples, a 16-stage cascade classifier for cross detection was trained. Following the same procedure, the detectors for sandglass and rhombus shapes could be derived as well.

D. Codeword Retrieval

By using the pre-trained primitive shape detectors, the centroid of each primitive, i.e., the position of each feature point, can be determined. Once a feature point is extracted from the image, its codeword can be produced from the associated 3×3 intensity window centered on the feature point. As shown in Fig. 6, the codeword of P_0 is calculated as $CW = \sum_{i=0}^{8} 10^i \times C_i$, where C_i is the code of point P_i. It is time-consuming and inefficient for searching the primitive shapes in the whole image, the directional information embraced in the cross shape could rectify the search window around it to find the other two shapes. As illustrated in Fig. 6, the cross shapes are detected first, then two directions are fitted through the intensity distributions in the detected rectangle, and in the end, rhombus and sandglass shapes are detected in the nearby area along the two directions. The corresponding point on the projector image plane is known a priori. This way 3D position on the object surface can be determined via triangulation. The above is the 3D sensing step we use in the system.

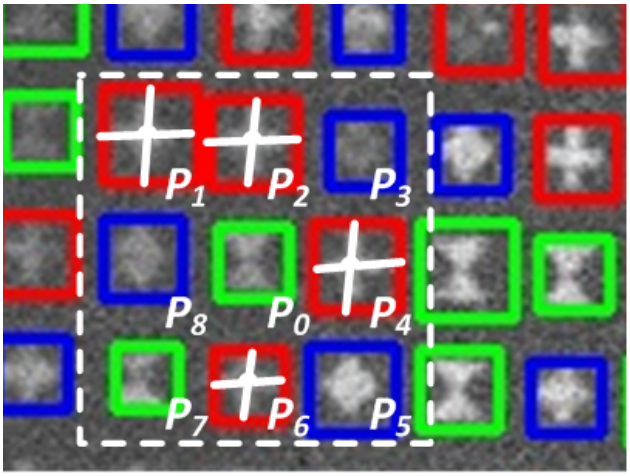

Fig. 6. An example of codeword retrieval.

IV. EXPERIMENTS

A. Overview of Experiment Setup

To assess the feasibility of the proposed method for embedding imperceptible codes in regular projection, we conducted experiments on embedded code imperceptibility evaluation, primitive shape detector accuracy evaluation and primitive shape detector sensitivity evaluation.

In order to evaluate the performance of our method in different platforms, we set up two projector-camera systems using different equipment. The first one (*PROCAMS-A*) consisted of a consumer-level DLP projector (Mitsubishi EX240U projector) of 1024×768 resolution and $120Hz$ refresh rate, and a CMOS camera (Point Grey Flea 3 FL3-U3-13S2C with Myutron FV1520 f15mm lens) of 1328×1048 resolution and $120fps$, while the second one (*PROCAMS-B*) consisted of a Pico DLP projector with a native resolution of 640×480 and an interface for firmware

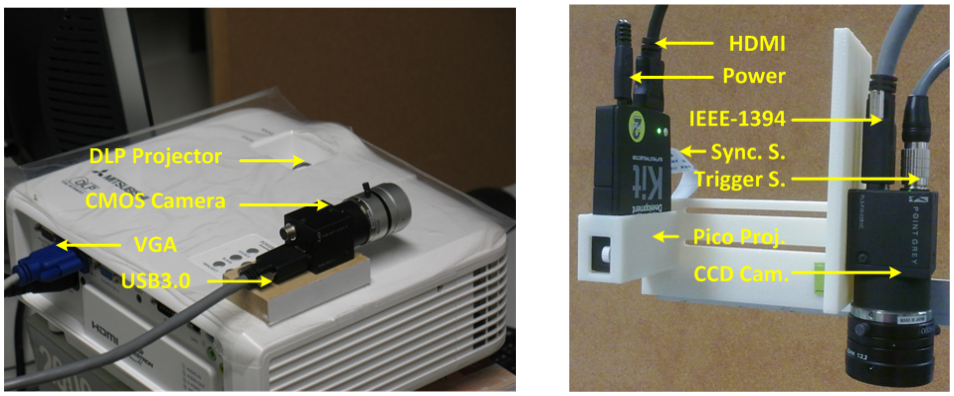

(a) PROCAMS-A (b) PROCAMS-B

Fig. 7. Hardware configuration of two projector-camera systems.

configuration (TI DLP Pico Projector Development Kit 2), plus a CCD camera of 648×488 resolution at $120fps$ (Point Grey FL3-FW-03S1C camera with Myutron FV0622 f6mm lens).

For *PROCAMS-A*, we first fixed the camera and projector rigidly, and the projector and camera were connected to a desktop computer through VGA and USB3.0 interfaces respectively. Since there was no synchronization signal output in the consumer-level projector, the synchronization between projectors and cameras was implemented through software delay. The hardware configuration is shown in Fig. 7(a). For *PROCAMS-B*, the projector and camera were mounted on a special designed framework rigidly, and were connected to a laptop computer through HDMI and IEEE-1394 interfaces respectively, and the hardware trigger signal of the camera was connected to the sync. output of the projector for synchronization between them, which are illustrated in Fig. 7(b).

Moreover, the projector-camera systems were calibrated using an LCD monitor as the calibration object; the calibration method, detailed in [24], could derive the intrinsic and extrinsic parameters of the two instruments. Once the experimental system was set up and calibrated, we could conduct further experiments.

B. Embedded Code Imperceptibility Evaluation

Embedded code imperceptibility and user satisfaction are of the first priority in the system design. The imperceptibility depends on the embedded intensity. We conducted a subjective evaluation using *PROCAMS-A* based on a questionnaire. Ten persons were invited to participate in this experiment, of which six were male and four were female, and seven wearing glasses. Another 500 images were collected from Google Image [22] randomly, the content of the images included natural scene, portrait, architecture, animals and so on. Our proposed pattern was embedded into all the collected images with different intensities. The viewers were seated in front of a white planar screen at a distance of about $1m$, and asked to comment on the images projected to the screen. The questions asked were simplified from the questionnaire in [6], focusing on the feeling of flickering, the recognition of image deterioration, and the overall satisfaction for projection quality. The score for each question was divided into 10 levels.

The average scores of the subjective evaluation are illustrated in Fig. 8. When the embedded intensity is small, i.e., $\Delta = 5, 10$, the viewer could rarely notice the embedded codes and were satisfied with the projection quality. With the increase of the embedded intensity, the viewers' sense of flickering and image degradation became stronger. When $\Delta = 25$, almost every viewer was not satisfied with the projection quality.

In practice, because it was difficult to retrieve weakly embedded codes with the standard commercial cameras, we choose $\Delta = 10$ in our configuration, striking a compromise between user satisfaction and code imperceptibility.

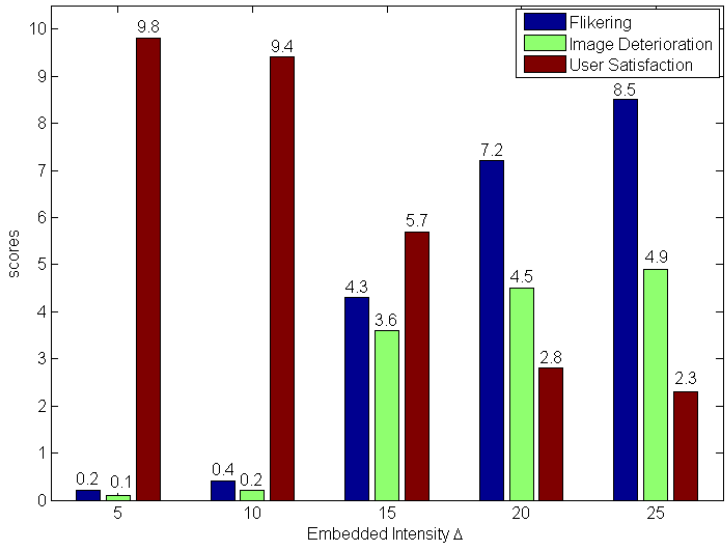

Fig. 8. Subjective evaluation results for code imperceptibility.

C. Primitive Shape Detection Accuracy Evaluation

After embedded code imperceptibility evaluation, the experiments for primitive shape detection accuracy were carried out. Considering the training data for primitive shape detector training was collected by *PROCAMS-A*, we first evaluated the primitive shape detection accuracy on *PROCAMS-A*.

To assess accuracy, the experimental data with ground-truth were required. Three different primitives and the spatially coded pattern image were embedded into 500 images used for imperceptibility evaluation respectively, with intensity $\Delta = 10$. Then the projected and complementary images were projected successively to a projection surface, while the camera conducted synchronized capture. The projection surface was the same as the one used for training data collection. Then the subtraction images embracing embedded codes information were derived for accuracy evaluation. The ground-truth was obtained by manual labeling in the image data captured under binary pattern illumination.

Experimental results in some subtraction images are presented in Fig. 9. The four sub-figures display the cross (top-left), sandglass (top-right), rhombus (bottom-left) shapes, and the spatially coded pattern (bottom-right) respectively. For qualitative evaluation, the detected features are indicated by rectangles, and in the bottom-right

sub-figure, the cross, sandglass and rhombus shapes are separately marked by red, green and blue rectangles. The accuracy of primitive detector are evaluated by hit rate (H), missing rate (M), false rate (F) and position error (E_d), which are formulated as

$$H = \frac{N_h}{N_t}, \tag{5}$$

$$M = \frac{N_m}{N_t}, \tag{6}$$

$$F = \frac{N_f}{N_t}, \tag{7}$$

$$E_d = \sqrt{\epsilon_X^2 + \epsilon_Y^2}, \tag{8}$$

$$\epsilon_X = \frac{1}{N_h}\sum_{i=1}^{N} |X_d - X_g|_i, \tag{9}$$

$$\epsilon_Y = \frac{1}{N_h}\sum_{i=1}^{N} |Y_d - Y_g|_i, \tag{10}$$

where N_t is the total embedded primitive shape number, N_h, N_m and N_f are the number of correct detections, missed detections and false detections respectively. ϵ_X and ϵ_Y are the average feature point detection errors along the x-axis and y-axis, (X_d, Y_d) and (X_g, Y_g) are the detected coordinate and ground-truth respectively.

The more detailed quantitative testing results are listed in Table I. Through the proposed method, 95.74% of the embedded feature points could their correspondences found correctly. By analyzing the missed and false detection cases, we find that the mistakes were mainly caused by large noise that occludes the embedded codes, implying that external noise has the greatest influence on the decoding process.

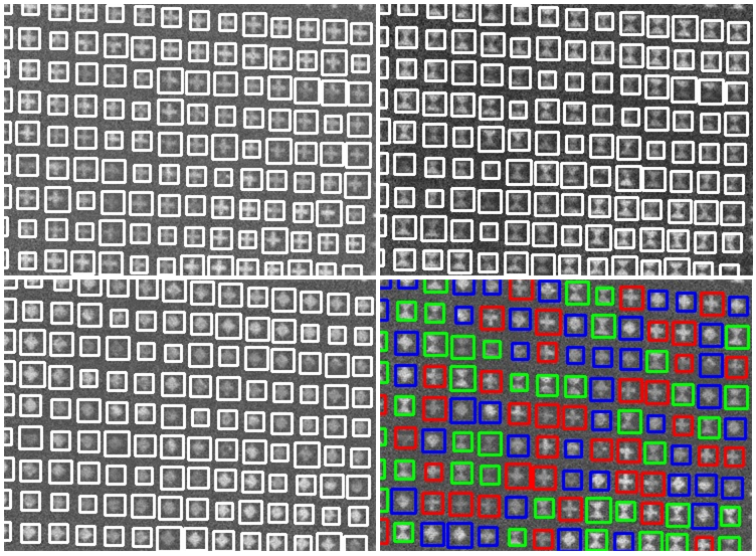

Fig. 9. Some qualitative experiment results on accuracy evaluation.

	H(%)	M(%)	F(%)	E_d(pixel)	Corr. Acc.(%)
Cross	94.53	3.95	1.52	1.632	—
Rhombus	95.21	3.59	1.20	1.833	—
Sandglass	95.50	3.63	0.87	1.542	—
Whole Pattern	92.11	11.06	5.28	2.013	95.74

TABLE I
BENCHMARK FOR SENSITIVITY EVALUATION.

V. SENSITIVITY EVALUATION

It is obvious that the performance of our method depends on the performance of pre-trained primitive shape detectors, which is determined by the training process to a great extent. Generally, for the training based methods, generalization of the training results is an issue, especially, when the scenarios between training stage and operation stage are quite different.

In the framework of our method, due to the different sensor-object localization, different projection surfaces, different surrounding environment and different hardware platforms, the generalization of the pre-trained detector is of great importance, since it is both impractical and impossible to re-train the detector for different scenarios. It is necessary to certify the validity of our method in different application scenarios.

In this section, we will evaluate the the sensitivity of primitive detectors under different circumstances, including variations on working distance, projection surface orientation, projection surface shape, projection surface texture and hardware configuration. Since the settings of accuracy evaluation in Section IV-C are the same as training sample collection stage, the results are considered as the benchmark for sensitivity evaluation.

A. Working Distance

The working distance is the average distance from the projector-camera system to the object surface. When the intrinsic parameters of the projector and camera (focal length and resolution) are fixed, the size of the primitive shapes in subtraction image data is determined by the working distance directly. In the configuration of training stage, the working distance is set as $800mm$, the size of primitive shapes in image data is about 20 pixels. In the operation stage, the working distance is changed to $500mm$, $1200mm$ and $1600mm$, the focal length of procams is slightly adjusted to get sharp projection and clear capture. Some subtraction images with detection results are shown in Fig. 10; the size of the primitive shapes are around 15, 35 and 45 pixels respectively.

The detailed quantitative results are listed in Table II. It is clear that when the working distance decreased to $500mm$, the hit rates dropped, because it is difficult for primitive shape detectors to find small size shapes in image data. For the enlarged shapes in larger working distance, the performance of detectors are almost the same as those of the benchmark.

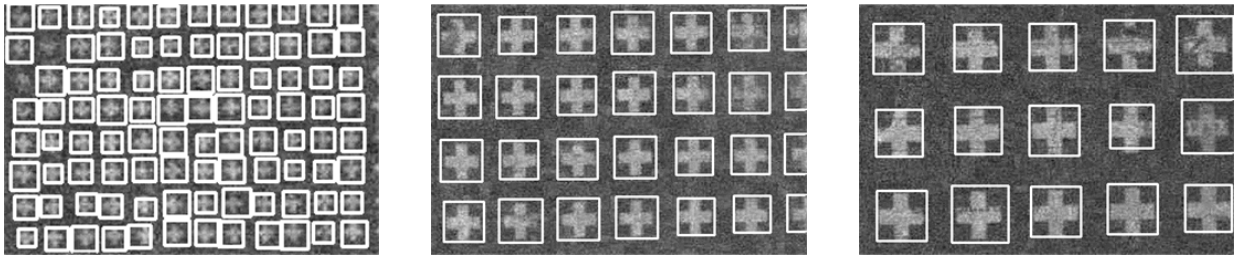

(a) $500mm$ (b) $1200mm$ (c) $1600mm$

Fig. 10. Cross shape detection in different working distances.

TABLE II

PRIMITIVE SHAPE DETECTION ACCURACY IN DIFFERENT WORKING DISTANCES.

Distance	Primitive	Hits(%)	Missed(%)	False(%)	E_d(pixel)
$500mm$	Cross	86.21	11.63	2.16	1.814
	Rhombus	85.83	12.57	1.60	1.836
	Sandglass	87.49	11.64	0.87	1.712
$1200mm$	Cross	94.44	4.32	1.24	1.728
	Rhombus	94.86	4.23	0.91	1.904
	Sandglass	94.49	4.62	0.89	1.572
$1600mm$	Cross	94.52	4.11	1.37	1.731
	Rhombus	95.06	3.92	1.02	1.910
	Sandglass	95.39	3.68	0.93	1.591

B. Projection Surface Orientation

Besides the size of the primitive shapes in image data, the distortions will also influence the performance of the pre-trained detectors. The distortions mainly come from the variations on the orientation of the projection surface with respect to the sensing system and the variations on the shape of the projection surface. First, the detector accuracy will be evaluated under different projection surface orientations.

In the training data collection stage, the images were projected to a planar surface that is almost parallel to the image plane of the camera. Now in the operation stage, the orientation of the surface is adjusted to 10°, 20°, 30°, 40°, 50° in the yaw direction, as shown in Fig. 11. In each sub-image, the upper part is the captured image to show the extent of distortion, while the lower part is the magnified subtraction image of the subregion indicated by the rectangle in captured image. The detection results are also shown in the subtraction images. More detailed quantitative results are listed in Table III.

In the testing results, when the rotation degree θ is small, i.e., $\theta = 10^\circ, 20^\circ$, the performance is almost the same as those of the benchmark. With the increase of the rotation degree, the hit rates decrease slightly. When $\theta = 50^\circ$, more than 85% primitive shapes are still detected correctly, which satisfies the application requirements.

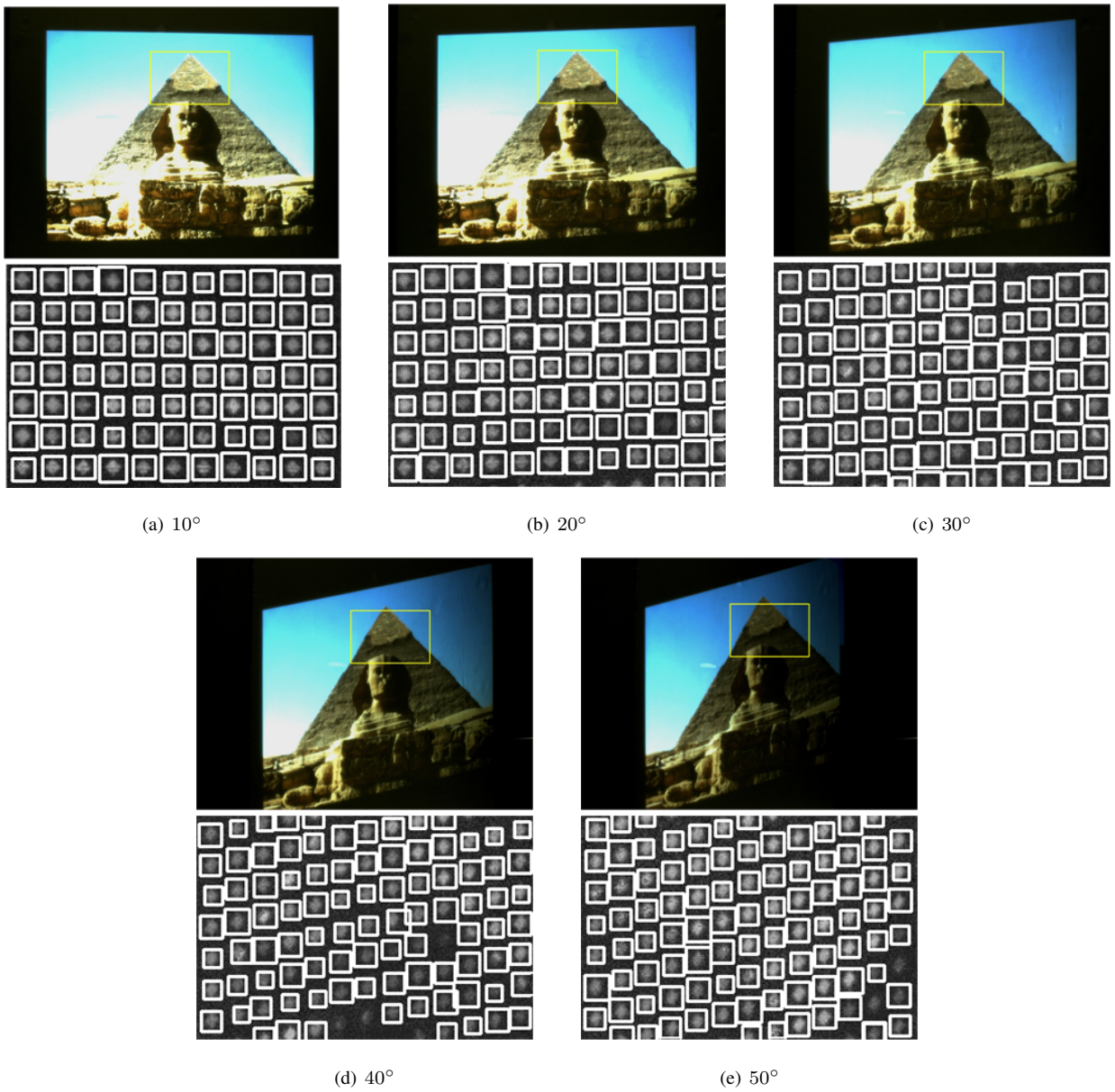

(a) 10° (b) 20° (c) 30°

(d) 40° (e) 50°

Fig. 11. Rhombus shape detection in the projection surface under different orientations.

C. Projection Surface Shape

The alteration of projection surface shape will also result in the distortion of primitive shapes in the image data. In the training stage, the negative and positive sample were collected from the images projected to a planar surface. In this test, the projection surface are three different non-planar surfaces (convex paper, concave paper and plaster statue). Some test images and the statistical results are shown in Fig. 12 and Table IV respectively. In all three surfaces, although the hit rates have small decrease, it is still sufficient to derive correct correspondences for triangulation. In the plaster statue case, the missing detections are mainly found in the regions where the surface

TABLE III

PRIMITIVE SHAPE DETECTION ACCURACY UNDER DIFFERENT SURFACE ORIENTATIONS.

Orientation	Shape	Hits(%)	Missed(%)	False(%)	E_d(pixel)
10°	Cross	94.51	3.96	1.53	1.635
	Rhombus	95.08	3.60	1.22	1.845
	Sandglass	95.46	3.74	0.80	1.544
20°	Cross	94.50	3.96	1.54	1.634
	Rhombus	95.08	3.64	1.08	1.848
	Sandglass	95.43	3.77	0.80	1.564
30°	Cross	93.47	4.50	2.03	1.938
	Rhombus	92.15	6.37	1.48	2.141
	Sandglass	92.43	6.78	0.79	2.011
40°	Cross	90.19	7.70	2.11	2.414
	Rhombus	89.42	9.50	1.08	2.809
	Sandglass	91.23	7.87	0.90	2.374
50°	Cross	85.91	12.03	2.06	2.728
	Rhombus	85.48	12.81	1.71	2.904
	Sandglass	86.87	12.27	0.86	2.572

has sudden change.

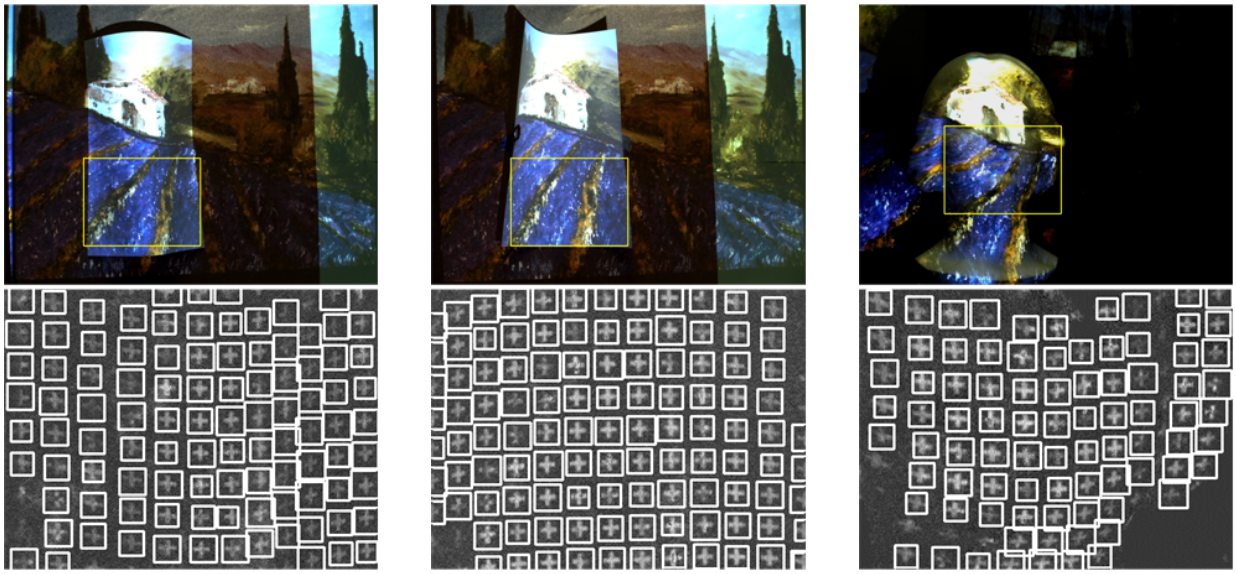

(a) Convex Paper (b) Concave Paper (c) Plaster Statue

Fig. 12. Cross shape detection from different projection surfaces.

TABLE IV

PRIMITIVE SHAPE DETECTION ACCURACY FROM PROJECTION SURFACES OF DIFFERENT SHAPES.

Surface	Shape	Hits(%)	Missed(%)	False(%)	E_d(pixel)
Convex Paper	Cross	93.53	4.86	1.61	1.756
	Rhombus	93.25	5.29	1.46	2.043
	Sandglass	94.14	4.85	1.01	2.122
Concave Paper	Cross	93.64	4.84	1.52	1.762
	Rhombus	93.82	4.70	1.48	2.108
	Sandglass	93.76	5.41	0.83	2.135
Plaster Statue	Cross	84.81	13.33	1.86	2.028
	Rhombus	85.73	13.06	1.21	1.904
	Sandglass	86.09	13.03	0.88	2.075

D. Projection Surface Texture

The texture on the projection surface will affect the quality of captured images. In the benchmark training stage, the projection surface is texture-free and in white color. In the operation stage (this test), the images are projected to a planar surface in green color, a cork board and a poster with text and images, as illustrated in Fig. 13. The quantitative results are listed in Table V. The results indicate that the texture variation on the projection surface has little influence on the performance of the primitive shape detectors, since in our method the decoding process was conducted in the subtraction image, which reduces the texture's influence substantially.

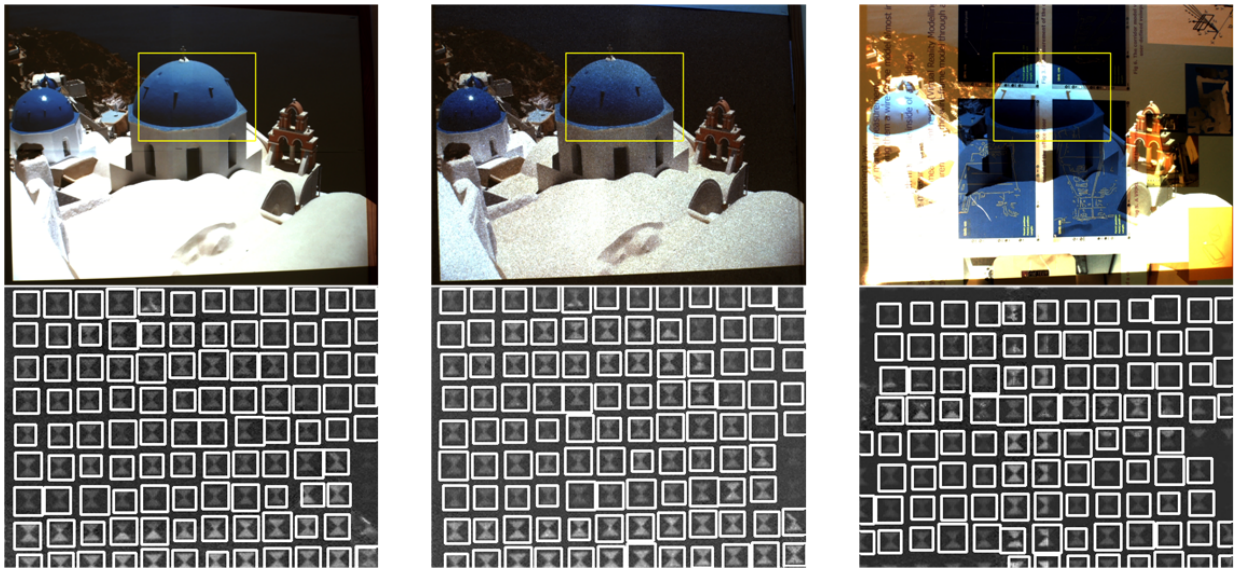

(a) Green paper (b) Cork board (c) Poster

Fig. 13. Sandglass shape detection in different projection surface textures.

TABLE V

PRIMITIVE SHAPE DETECTION ACCURACY IN DIFFERENT PROJECTION SURFACE TEXTURE.

Texture	Shape	Hits(%)	Missed(%)	False(%)	E_d(pixel)
Green Paper	Cross	94.41	4.17	1.42	1.634
	Rhombus	95.19	3.66	1.15	1.836
	Sandglass	95.49	3.63	0.88	1.558
Cork Board	Cross	93.41	5.07	1.52	1.641
	Rhombus	94.25	4.43	1.32	1.850
	Sandglass	94.92	4.16	0.92	1.623
Poster	Cross	91.74	6.63	1.63	2.024
	Rhombus	90.28	8.25	1.47	1.996
	Sandglass	92.19	6.76	1.05	1.762

TABLE VI

PRIMITIVE SHAPE DETECTION ACCURACY IN PROCAMS-B WITH DIFFERENT EMBEDDING APPROACHES.

	Shape	Hits(%)	Missed(%)	False(%)	E_d(pixel)
Cropped Pattern	Cross	80.23	14.43	5.34	3.028
	Rhombus	79.93	14.17	5.92	2.981
	Sandglass	81.09	13.28	5.63	2.812
Resized Pattern	Cross	30.52	59.23	10.25	2.628
	Rhombus	30.63	58.03	11.34	2.913
	Sandglass	30.80	57.93	11.27	2.874

E. Projector-Camera System

If the pre-trained detectors are used in another application with different hardware configuration, the performance of the detectors would be affected, since the differences in the resolution of the projector and camera (high versus low), the camera sensor (CCD versus CMOS), and the optical parameters (different lenses) will change the appearance of the primitive shape in the image data. In this test, the primitive detectors trained by the data collected from *PROCAMS-A* were applied to *PROCAMS-B* in the operation stage.

Due to the low projector resolution in *PROCAMS-B*, the dimension of the original pattern image was too large for embedding. We employed two methods to solve the issue. The first one was to select a sub-region of the original pattern image as a new pattern image and the second one was to resize the original pattern image to coincide with the projector resolution. Some detection results in the subtraction images derived from the two different embedding methods are illustrated in Fig. 14(b) and 14(c). The quantitative results are also shown in Table VI.

Compared with the benchmark, it is obvious that the performance in *PROCAMS-B* degraded intensively, especially in the resized pattern case. By analyzing the missed and false detection cases, we found that the mistakes were mainly caused by large noise from the low luminance of the pico projector and the extremely small primitive shapes in the image data.

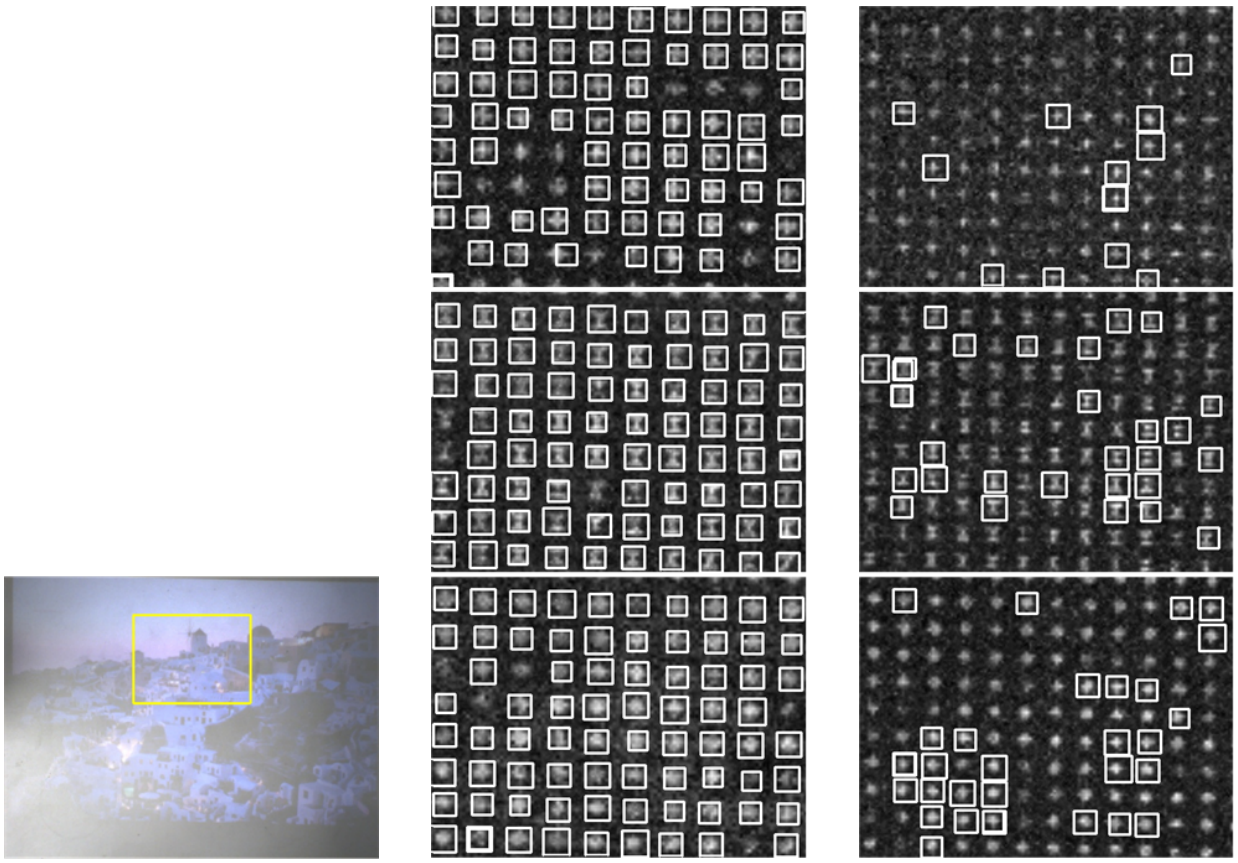

(a) Captured Image (b) Cropped Pattern (c) Resized Pattern

Fig. 14. Primitive shape detection in PROCAMS-B with different embedding approaches.

VI. Applications

The proposed method enables a common projector to serve the dual role of a display device as well as a 3D sensor, which can be extended or integrated to many applications. In this section, we will show three cases to demonstrate the feasibility of our method.

A. 3D Reconstruction with Regular Video Projection

3D reconstruction is the most straightforward application for structured light based sensing. To show the effectiveness of our method in 3D reconstruction task, we compared our method with the general structured light method that uses visible patterns.

As shown in Fig. 15-(a1)(b1)(c1) and Fig. 15-(a2)(b2)(c2), three objects (sphere, cone and cylinder) with known dimensions were illuminated by visible binary pattern image (the same as Fig. 4) and code embedded normal projection respectively.

In the general structured light scenario, feature points were extracted by segmentation and shape identification using the method proposed in [20], whilst in our code embedded regular projection scenario, feature points were

TABLE VII

COMPARISON OF 3D RECONSTRUCTION ACCURACIES.

Object	General SL [20]		Our Method	
	$E_\mu(mm)$	$E_\sigma(mm)$	$E_\mu(mm)$	$E_\sigma(mm)$
Sphere	1.502	0.576	1.410	0.587
Cylinder	2.054	0.824	1.939	0.762
Cone	1.383	0.557	1.391	0.564

detected and classified through the pre-trained primitive shape detectors. The depth value of each feature point was calculated through triangulation using the intrinsic and extrinsic parameters of projector and camera. Then on the basis of point clouds calculated through our method, surfaces were rendered as illustrated in Fig. 15-(a3)(b3)(c3). Since the dimensions of the objects were known, we could conduct quantitative accuracy assessment. The residual mean error E_μ and standard deviation E_σ of the calculated 3D points with respect to ground-truth are listed in Table VII. It is evident that our method has almost the same performance as that of the general structured light method in 3D reconstruction. By the reason that textures on the cylindrical object obstruct code retrieval, the reconstruction error on the cylindrical object is greater than those of the other two objects. It is worth pointing out that in our method the decoding process was conducted in the subtraction image, which would reduce the texture influence.

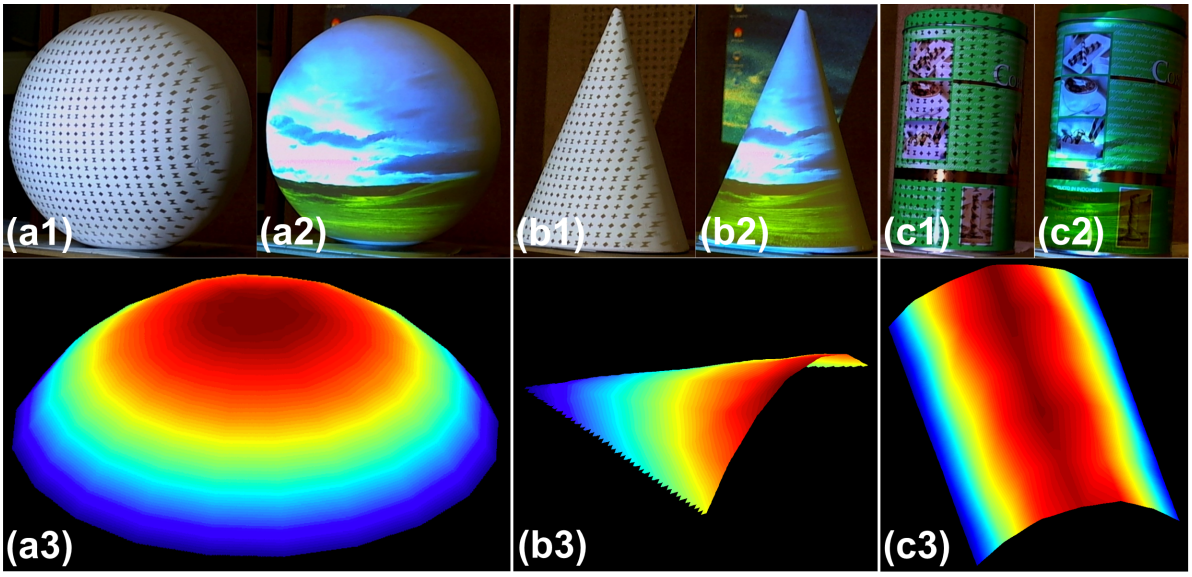

Fig. 15. Some results of 3D reconstruction.

B. Sensing Surrounding Environment on Mobile Robot Platform

For the purpose of illustrating the proposed method's potential applications in robotic system working in varied environment, we mounted a projector and a camera rigidly on a specially designed frame, and fixed the frame to a tripod affixed to a mobile robot manufactured by ARRICK Robotics [25], as shown in Fig. 16.

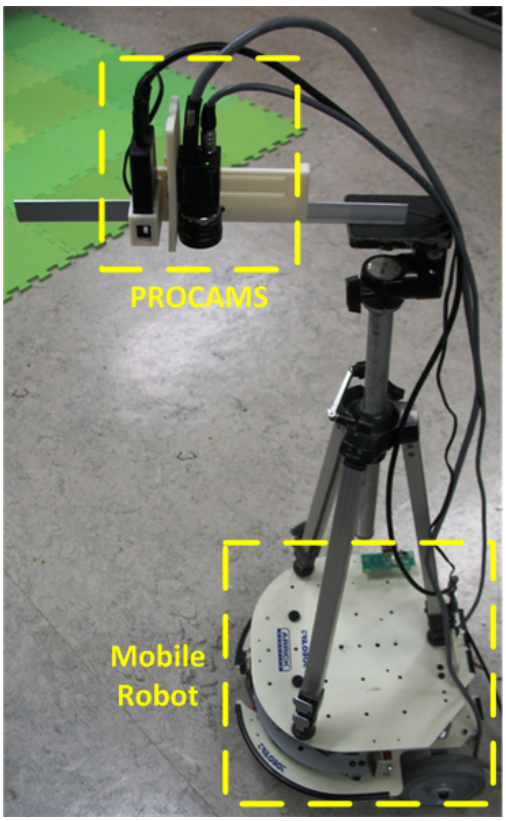

Fig. 16. Integration with mobile robot system.

For a mobile robot, one of the essential capabilities is to sense the surrounding environment for navigation, obstacle avoidance, object recognition and some other purposes. We assist the visual sensing through a normal grey illumination with invisible codes embedded. By retrieving the embedded codes, correspondences between projection plane and image plane could be established accurately and efficiently. In Fig. 17 (a) and (c), a green tea can and toy bricks were located in the illumination area of the projector, and 3D depth information of certain points on the objects was acquired through simple triangulation in real-time. The surfaces of the objects were rendered in 3D as shown in Fig. 17 (b) and (d). Although the ground truth of the objects was not available, qualitative examination showed that the reconstructed surfaces were of reasonable quality.

C. Natural Human-Computer Interaction

Besides sensing capabilities, the mobile robot should also provide an effective channel for the interaction between users, such as an interface for system configuration or a display panel to show prompt information. Traditionally,

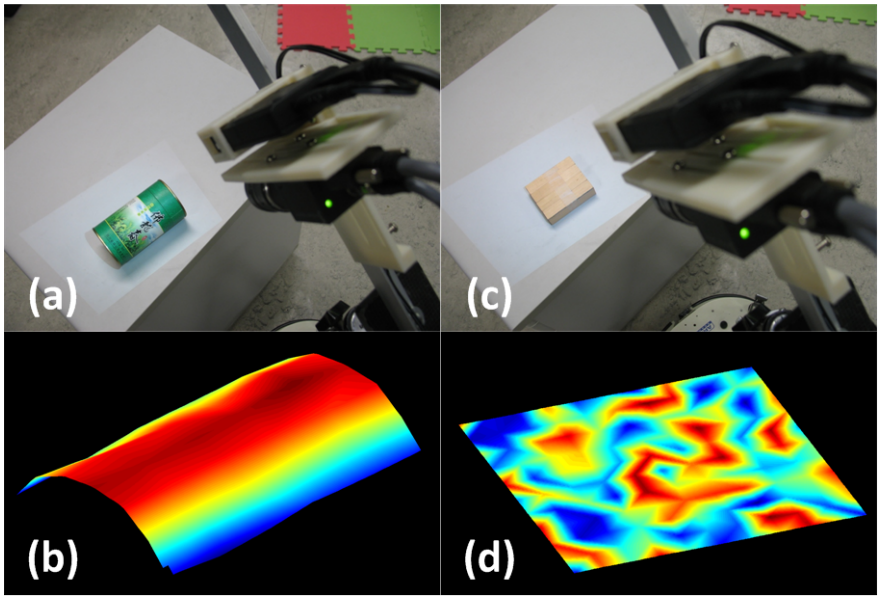

Fig. 17. Some 3D sensing results.

an LCD monitor plus mouse-and-keyboard or an LCD touch-screen attached to the robot is used, which would inevitably increases the weight and size of the mobile robot, plus energy consumption. Our method enables a common projector to serve the dual role of a display device as well as a 3D sensor with the assistance of camera, providing a platform for more natural user interface schemes. As shown in Fig. 18 (a), a system configuration interface (Fig. 18 (b)) was projected onto a desk surface, and a user was operating on the projected desk surface with bare-hand (Fig. 18 (c)). From an image alone, say of a finger on top of a table surface, one cannot tell whether the finger is actually touching the table surface or not. The case of a finger hanging in air, and the case of a finger touching the table surface, could both produce the same image to the camera. By incorporating the structured light invisible embedded into the projection, 3D acquisition can be made possible, and contact identification and finger movement recognition could be readily tackled[2]. It is possible to convert any textureless light color plane (table-surfaces, whiteboards or walls) to a touching sensitive screen, providing more natural and flexible interface for bare-hand human-robot interaction.

VII. CONCLUSION AND FUTURE WORK

We have described a novel system of embedding imperceptible structured codes into normal projection that strikes the balance between imperceptibility and detectability of the codes. Through precise projector-camera synchronization, structured codes consisting of three primitive shapes are embedded into regular projection, in a way that is imperceptible to the user but extractable by a camera (through the ”difference image” between successive

[2]We have implemented fingertip touching detection method under invisible codes embedded illumination, but this is to be detailed in another article due to the-space constraint.

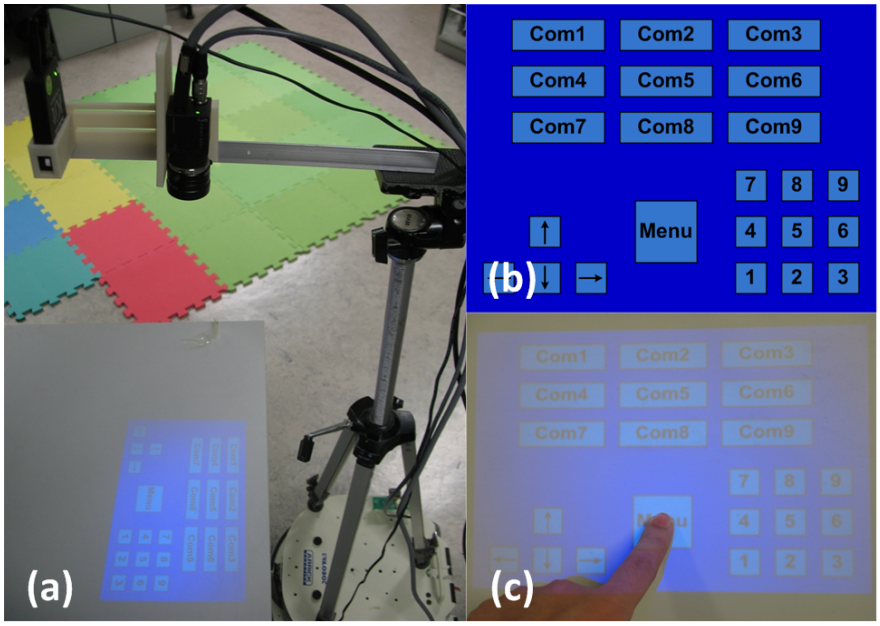

Fig. 18. Touch-sensitive user interface on projection surface.

images). The disturbances caused by external noise make it difficult to retrieve the codes by the region segmentation approaches adopted in general structured light based systems. Instead of segmenting the codes, specially trained classifiers are employed to detect and identify them. To increase the robustness of code extraction, large Hamming distance is adopted in spatial coding. Even if some bits are missed or wrongly decoded, the correct correspondence between the projection panel and the image plane could still be arrived at correctly for structured light sensing. Extensive evaluations shows that the method is a promising one.

In the current system, the image capture interval is $10ms$. In sensing object that moves fast, the substantial displacement between successive images will result in blur or destruction of the embedded codes in the difference image. Some compensation methods need be in place to deal with the issue. In addition, the embedded code could be denser for more precise 3D sensing. New coding scheme capable of generating denser patterns should be used. The proposed method enables a common projector to serve the dual role of a display device as well as a 3D sensor. That provides a platform for more natural user interface schemes. Our future work will lie on these directions.

VIII. ACKNOWLEDGMENT

This work is affiliated with the Microsoft-CUHK Joint Laboratory for Human-centric Computing & Interface Technologies.

REFERENCES

[1] J. Salvi, S. Fernandez, T. Pribanic and X. Llado, "A state of the art in structured light patterns for surface profilometry," *Pattern Recognition*, vol. 43, no. 8, pp. 2666–2680, 2010.

[2] O. Bimber, D. Iwai, G. Wetzstein and A. Grundhöfer, "The visual computing of projector-camera systems," in *ACM SIGGRAPH 2008 classes*, ser. SIGGRAPH '08, 2008, pp. 1–25.

[3] D. Fofi, T. Sliwa and Y. Voisin, "A comparative survey on invisible structured light," in *Proceedings of Machine Vision Applications in Industrial Inspection XII*, 2004, pp. 90–98.

[4] R. Raskar, G. Welch, M. Cutts, A. Lake, L. Stesin, and H. Fuchs, "The office of the future: A unified approach to image-based modeling and spatially immersive displays," in *Proceedings of SIGGRAPH 98*, 1998, pp. 179–188.

[5] D. Cotting, M. Naef, M. Cross and H. Fuchs, "Embedding imperceptible patterns into projected images for simultaneous acquisition and display," in *Proceedings of The IEEE and ACM International Symposium on Mixed and Augmented Reality*, 2004, pp. 100–109.

[6] Hanhoon Park, Byung-Kuk Seo and Jong-Il Park, "Subjective evaluation on visual perceptibility of embedding complementary patterns for nonintrusive projection-based augmented reality," *IEEE Transactions on Circuits and Systems for Video Technology*, vol. 20, no. 5, pp. 687 –696, 2010.

[7] Hanhoon Park, Moon-Hyun Lee, Byung-Kuk Seo, Yoonjong Jin and Jong-Il Park, "Content adaptive embedding of complementary patterns for nonintrusive direct-projected augmented reality," in *HCI international*, 2007, pp. 132–141.

[8] A. Grundhofer, M. Seeger, F. Hantsch and O. Bimber, "Dynamic adaptation of projected imperceptible codes," in *Proceedings of the 2007 6th IEEE and ACM International Symposium on Mixed and Augmented Reality*, 2007, pp. 1–10.

[9] K. L. Boyer and A. C. Kak, "Color-encoded structured light for rapid active ranging," *IEEE Transactions on Pattern Analysis and Machine Intelligence*, vol. 9, no. 1, pp. 14–28, 1987.

[10] J. Salvi, J. Batlle, and E. Mouaddib, "A robust-coded pattern projection for dynamic 3d scene measurement," *Pattern Recognition Letters*, vol. 19, no. 11, pp. 1055–1065, 1998.

[11] J. Pages, J. Salvi, and J. Forest, "A new optimised de bruijn coding strategy for structured light patterns," in *Proceedings of the 17th International Conference on Pattern Recognition*, vol. 4, 2004, pp. 284–287.

[12] T. Etzion, "Constructions for perfect maps and pseudorandom arrays," *IEEE Transactions on Information Theory*, vol. 34, no. 5, pp. 1308–1316, 1988.

[13] H. Morita, K. Yajima, and S. Sakata, "Reconstruction of surfaces of 3-d objects by m-array pattern projection method," in *Proceedings of Second International Conference on Computer Vision*, 1988, pp. 468–473.

[14] R. Morano, C. Ozturk, R. Conn, S. Dubin, S. Zietz, and J. Nissano, "Structured light using pseudorandom codes," *IEEE Transactions on Pattern Analysis and Machine Intelligence*, vol. 20, no. 3, pp. 322–327, 1998.

[15] J. Pages, C. Collewet, F. Chaumette, and J. Salvi, "An approach to visual servoing based on coded light," in *Proceedings of 2006 IEEE International Conference on Robotics and Automation*, 2006, pp. 4118–4123.

[16] M. Maruyama and S. Abe, "Range sensing by projecting multiple slits with random cuts," *IEEE Transactions on Pattern Analysis and Machine Intelligence*, vol. 15, no. 6, pp. 647–651, 1993.

[17] P. Fechteler and P. Eisert, "Adaptive colour classification for structured light systems," *IET Computer Vision*, vol. 3, no. 2, pp. 49–59, 2009.

[18] T. Koninckx and L. Van Gool, "Real-time range acquisition by adaptive structured light," *IEEE Transactions on Pattern Analysis and Machine Intelligence*, vol. 28, no. 3, pp. 432–445, 2006.

[19] H. Hiroshi Kawasaki, R. Furukawa, R. Sagawa, and Y. Yagi, "Dynamic scene shape reconstruction using a single structured light pattern," in *Proceedings of IEEE Conference on Computer Vision and Pattern Recognition*, 2008, pp. 1–8.

[20] C. Albitar, P. Graebling and C. Doignon, "Robust structured light coding for 3d reconstruction," in *Proceedings of IEEE 11th International Conference on Computer Vision*, 2007, pp. 1–6.

[21] P. Viola and M. Jones, "Rapid object detection using a boosted cascade of simple features," in *Proceedings of the 2001 IEEE Computer Society Conference on Computer Vision and Pattern Recognition*, vol. 1, 2001, pp. 511–518.

[22] "Google image," http://images.google.com/, accessed: 30/08/2012.

[23] R. Lienhart, A. Kuranov and V.Pisarevsky, "Empirical analysis of detection cascades of boosted classifiers for rapid object detection," in *In DAGM 25th Pattern Recognition Symposium*, 2003, pp. 297–304.

[24] Z. Song and R. Chung, "Use of LCD panel for calibrating structured-light-based range sensing system," *IEEE Transactions on Instrumentation and Measurement*, vol. 57, no. 11, pp. 2623–2630, 2008.

[25] "ARRICK robotics," http://www.arrickrobotics.com/, accessed: 30/08/2012.